ACADEMIC PRESS

Available online at www.sciencedirect.com

SCIENCE DIRECT®

Journal of Magnetic Resonance 163 (2003) 163–173

JMR Journal of Magnetic Resonance

www.elsevier.com/locate/jmr

Measurement of ^{15}N chemical shift anisotropy in a protein dissolved in a dilute liquid crystalline medium with the application of magic angle sample spinning

Jun-ichi Kurita,[a] Hideto Shimahara,[a] Naoko Utsunomiya-Tate,[b] and Shin-ichi Tate[a,c,*]

[a] *Center for New Materials, Japan Advanced Institute of Science and Technology (JAIST), 1-1 Asahidai, Tatsunokuchi, Ishikawa 923-1292, Japan*
[b] *Department of Veterinary Science, Nippon Veterinary and Animal Science University, 1-7-1 Kyounan-cho, Musashino-shi, Tokyo 180-8602, Japan*
[c] *Department of Structural Biology, Biomolecular Engineering Research Institute (BERI), 6-2-3 Furuedai, Suita, Osaka 565-0874, Japan*

Received 13 December 2002; revised 25 February 2003

Abstract

The chemical shifts of nuclei that have chemical shielding anisotropy, such as the ^{15}N amide in a protein, show significant changes in their chemical shifts when the sample is altered from an isotropic state to an aligned state. Such orientation-dependent chemical shift changes provide information on the magnitudes and orientation of the chemical shielding tensors relative to the molecule's alignment frame. Because of the extremely high sensitivity of the chemical shifts to the sample conditions, the changes in chemical shifts induced by adding aligned bicelles do not arise only from the protein alignment but should also include the accumulated effects of environmental changes including protein–bicelle interactions. With the aim of determining accurate ^{15}N chemical shielding tensor values for solution proteins, here we have used magic angle sample spinning (MAS) to observe discriminately the orientation-dependent changes in the ^{15}N chemical shift. The application of MAS to an aligned bicelle solution removes the torque that aligns the bicelles against the magnetic field. Thus, the application of MAS to a protein in a bicelle solution eliminates only the molecular alignment effect, while keeping all other sample conditions the same. The observed chemical shift differences between experiments with and without MAS therefore provide accurate values of the orientation-dependent ^{15}N chemical shifts. From the values for ubiquitin in a 7.5% (w/v) bicelle medium, we determined the ^{15}N chemical shielding anisotropy (CSA) tensor. For this evaluation, we considered uncertainties in measuring the ^{1}H–^{15}N dipolar couplings and the ^{15}N chemical shifts and also structural noise present in the reference X-ray structure, assuming a random distribution of each NH bond vector in a cone with 5° deviation from the original orientation. Taking into account these types of noise, we determined the average ^{15}N CSA tensor for the residues in ubiquitin as $\Delta\sigma = -162.0 \pm 4.3$ ppm, $\eta = 0.18 \pm 0.02$, and $\beta = 18.6 \pm 0.5°$, assuming a ^{1}H–^{15}N bond length of 1.02 Å. These tensor values are consistent with those obtained from solid-state NMR experiments.

Keywords: Magic angle spinning; Weak alignment; Chemical shift anisotropy; Residual dipolar coupling; Bicelle

1. Introduction

The change in chemical shift observed for a given nucleus with anisotropic nuclear shielding, when shifting from an isotropic medium to a liquid crystalline phase, gives information on the magnitude and orientation of chemical shift anisotropy (CSA) tensor relative to the molecular alignment frame [1–4]. Accurate knowledge of the CSA tensor values is essential for the quantitative interpretation of backbone dynamics in spin relaxation analyses, especially when considering the anisotropic overall tumbling motion [5–9]. For the interpretation of experiments using the interference between CSA and dipolar interactions, the CSA tensor angles are also required [10,11].

In addition to solid-state NMR experiments [12–23], several trials using liquid-state NMR to determine the ^{15}N CSA tensors have been reported recently [1,3,4,24–28]. In liquid-state experiments, the magnetic field dependence of the ^{15}N relaxation rate yielded a considerably lower CSA value [27], $\Delta\sigma = -172 \pm 13$ ppm, than

* Corresponding author. Fax: +81-6-6872-8210.
E-mail address: tate@beri.or.jp (S.-i. Tate).

1090-7807/03/$ - see front matter © 2003 Elsevier Science (USA). All rights reserved.
doi:10.1016/S1090-7807(03)00080-6

that observed in solid-state experiments, $\Delta\sigma = -160$ ppm. Independent support for this lower value was provided from a ^{15}N dipolar–CSA relaxation interference experiment [28], $\Delta\sigma = -170$ ppm, and also from measuring changes in the ^{15}N chemical shifts that occurred when a protein was partially oriented in the magnetic field [4], $\Delta\sigma = -168 \pm 20$ ppm. Different approaches using orientation-dependent chemical shift changes under enhanced alignment by bicelles also support the lower ^{15}N CSA value [1,3]. These two experiments used temperature shifts over the phase-transition point for the bicelle medium, during which the bicelle is switched from an isotropic to a liquid crystalline phase [1,3]. Cornilescu and Bax [3] reported a value of $\Delta\sigma = -162.5$ ppm with a vibrationally corrected ^{1}H–^{15}N bond length 1.04 Å [29]. They also noted that the $\Delta\sigma$ value is lowered to -173 ppm if the static ^{1}H–^{15}N bond length, $r_{nh} = 1.02$ Å, is used [3], which is in good agreement with the $\Delta\sigma$ value from ^{15}N relaxation studies [27,28]. Boyd and Redfield [1] reported $\Delta\sigma = -174.4$ ppm, with the assumption of $r_{nh} = 1.04$ Å, further supporting the lower $\Delta\sigma$ value. However, Fushman and coworkers [24–26] have reported a different average $\Delta\sigma$ value, -157 ± 19 ppm, from ^{15}N relaxation measurements made at multiple fields.

The noted discrepancy for the reported ^{15}N CSA values among the various NMR experiments motivated us to determine the ^{15}N CSA tensor by an alternative method that enables us to obtain more accurate orientation-dependent changes in the ^{15}N chemical shifts, $\Delta\delta^{15}$N. In the present work, we applied magic angle spinning (MAS) to an aligned bicelle medium. The rapid sample spinning over the reorientation rate of the liquid crystalline bicelle at the magic angle, 54.7°, removes the torque that aligns the discoidal phospholipid against the magnetic field [30–33]. Thus, under MAS, the bicelles are not aligned, even though they maintain their discoidal shape and show negative magnetic susceptibility as potency for their alignment [30–33]. Therefore, the chemical shift differences in the spectra observed with and without MAS provide directly the orientation-dependent ^{15}N chemical shift changes. Because sample conditions other than the alignment are kept the same between the experiments carried out with and without MAS, we can measure more accurate orientation-dependent changes to the ^{15}N chemical shifts.

In the present calculation for the ^{15}N CSA tensor, in addition to the measuring uncertainties in the dipolar couplings and the chemical shifts, we also considered structural noise present in the reference X-ray structure, which was represented by a Gaussian random distribution of each NH bond vector in a cone with 5° deviation from its original orientation [34]. The obtained CSA values with errors, by assuming either $r_{nh} = 1.04$ Å or $r_{nh} = 1.02$ Å, were -162.0 ± 4.3 and -152.9 ± 4.1 ppm, respectively, for ubiquitin dissolved in a 7.5% (w/v) phospholipid bicelle medium at 30 °C. These values are in good agreement with those obtained by solid-state NMR and ^{15}N relaxation studies by Fushman and coworkers [24–26], but slightly larger than the values from other solution NMR experiments, in which $\Delta\sigma$ is around -170 ppm [1,3,4,27,28].

In this paper, we describe the details of these MAS, or so-called 'high-resolution MAS,' experiments for determining the ^{15}N CSA tensor. In addition, we report the ^{15}N CSA values determined with extensive noise consideration, including not only the error evaluation noted above but also possible systematic drift to the observed $\Delta\delta^{15}$N.

2. Experimental

2.1. Sample preparation

Uniformly ^{15}N-labeled human ubiquitin, whose gene was derived from HeLa cell, was used in the present experiments. The gene was subcloned into expression vector pET21. Protein expression from this construct in *Escherichia coli* strain BL21(DE3), uniform enrichment by ^{15}N, and protein purification by ion-exchange were carried out essentially as described previously [47]. The backbone resonance assignments under the present solution conditions were obtained using ^{13}C and ^{15}N double-labeled human ubiquitin expressed from our construct with standard triple-resonance experiments [48].

A bicelle mixture of dimyristoylphosphatidylcholine (DMPC) and dihexanoylphosphatidylcholine (DHPC) doped with cetyltrimethylammonium bromide (CTAB) was prepared according to a previously described procedure [35,37,49,50]. Here, we used a 3.2:1.0:0.1 DMPC:DHPC:CTAB 7.5% (w/v) bicelle solution containing 50 mM sodium phosphate pH 6.4 and 2 mM EDTA. The sample solution contained 0.5 mM ^{15}N-enriched human ubiquitin and 95% H_2O and 5% D_2O. The same sample solution was divided into 160 μl and 40 μl aliquots for spectral measurement in normal and MAS NMR experiments, respectively.

2.2. NMR spectroscopy

All spectra were recorded at 30 °C, at which the quadrupolar splitting observed in the ^{2}H NMR spectra of the sample solution was 10.9 Hz. The data in an aligned state were recorded with the ^{1}H-{X} double-resonance probe equipped with *Z*-axis gradient coil on a Varian INOVA500 spectrometer operating at 499.84 MHz for ^{1}H. For data collection under MAS, we used a Varian gHX NanoProbe harboring a ^{1}H-detection coil with X tuned for ^{15}N, equipped with a "magic angle" single axis gradient coil. The sample solution for

the experiments in an aligned state was poured into a Shigemi micro-cell (BMS-2, Shigemi). The 40 μl sample solution for the MAS experiment was packed into a Varian standard glass tube for the NanoProbe. The sample spinning rate was 2.6 kHz, which was enough to eliminate anisotropic spin interactions and also average out field inhomogeneity [45].

The ^{1}H–^{15}N dipolar couplings were measured in ^{1}H–^{15}N IPAP-HSQC spectra collected with the pulse scheme modified in the standard manner by attachment of pulsed-field gradient sensitivity enhancement [48]. The acquisition times in t_1 and t_2 dimensions were 111 and 128 ms, respectively, with the sizes of matrices $200 * (t_1, {}^{15}N) \times 1024 * (t_2, {}^{1}H)$ complex points. Apodization with 68°-shifted sine bell filters was used in both dimensions prior to extensive zero-filling to yield a digital resolution of 2.0 (^{1}H) and 0.88 Hz (^{15}N). For recording the ^{1}H–^{15}N HSQC 2D spectra, the ^{1}H–^{15}N HSQC with pulsed-field gradient sensitivity enhancement was used. The recorded data size and the applied data processing were the same as in the IPAP-HSQC spectra. Because of the limited sensitivity in the NanoProbe experiments, a greater number of scans was used to acquire data under MAS. In our experiments using 0.5 mM ^{15}N-labeled ubiquitin, 128 transients per one complex fid were applied to collect data under MAS. By contrast, for data collected with the standard probe, we used 32 transients per fid. All data were recorded on the same sample in a 7.5% (w/v) bicelle solution in an aligned condition at 30 °C.

Data were processed using the NMRpipe program software package [51]. Peak positions were determined by fitting ellipsoids to each of the calculated contours between 60 and 80% of the peak maximum with the program PIPP [52]. The center of each ellipsoid provides a measure for the peak position and values obtained for all contours in the 60–80% intensity range of a given peak were averaged to provide the peak position. This procedure improved the reproducibility of the measured peak positions [53].

2.3. Determination of alignment and CSA tensors

Inhouse-written C programs incorporating published subroutines [54] were used in this work to determine the alignment tensors and the ^{15}N CSA tensors. The alignment tensor can be derived from experimental dipolar couplings and a reference structure by singular value decomposition (SVD) [40]. The effect of experimental uncertainties in dipolar couplings and chemical shifts on best-fitted alignment tensor and CSA tensor was evaluated through iteration of the SVD calculation on the generated datasets. These datasets were generated by adding Gaussian noise to the experimental values. Gaussian noise was assumed to be distributed in a relative probability, $-\exp(x^2/2\sigma^2)$, where x is the experimental value and σ is the rms noise estimated from the pairwise rms deviation between successive measurements on either dipolar couplings or chemical shifts. The structural noise was simulated by reorienting the ^{1}H–^{15}N bond vectors in a random manner. The deviations between the original and the reoriented vectors are described in a cone having 5° tilt angle from the original orientation. In our simulation of structural noise, the tilt angles between the original and reoriented ^{1}H–^{15}N vectors were assumed to be in Gaussian distribution, $\exp(-\alpha^2/2\theta^2)$, where α is the tilt angle and θ is the assumed standard deviation for the tilt angle being fixed to 5° for this study. The transverse rotation angle of the re-reoriented vector in a cone was simulated to be equally distributed. The selection of the appropriate values from the simulated data was accomplished according to the criteria described in the text.

3. Results and discussion

3.1. Measurement of $^{1}D_{nh}$ and $\Delta\delta$

In this work, a 7.5% (w/v) DMPC/DHPC/CTAB ternary bicelle solution was used [35–37]. This ternary phospholipid bicelle has negative diamagnetic susceptibility, $\Delta\chi < 0$, in its discoidal liquid crystalline phase. In a high magnetic field, the director—the normal to the disk shape bicelle plane—orients perpendicular to the external magnetic field direction [30,31]. Fast sample spinning at greater than the critical frequency for the bicelle reorientation can incline the bicelle director from its energetically favorable direction in the stationary state [30–33]. The discoidal phospholipid shows different behavior for the director orientation depending on the range of the sample rotation angle, θ, from the magnetic field. In the range below the magic angle, $\theta < 54.7°$, the director tends to orient perpendicular to the rotation axis, whereas in the range above the magic angle, $\theta > 54.7°$, it orients parallel to the rotation axis [30–33]. At the exact magic angle, $\theta = 54.7°$, which is the switching point for the director orientation from perpendicular to parallel to the rotation axis, there is no torque to keep the director at a particular angle [33]. Thus, the overall order of the bicelle disappears under magic angle sample rotation (MAS), even though the discoidal shape is maintained and shows negative magnetic susceptibility. This was experimentally confirmed by the disappearance of the residual quadrupolar splitting for D_2O and the residual dipolar couplings for the protein dissolved in the bicelle medium under the MAS.

Fig. 1 shows a comparison of the ^{1}H–^{15}N HSQC spectra for ^{15}N-labeled ubiquitin in the bicelle medium in liquid crystalline phase measured with MAS (Fig. 1a) and without MAS (Fig. 1b). Elimination of the alignment of the bicelles by MAS caused significant ^{15}N

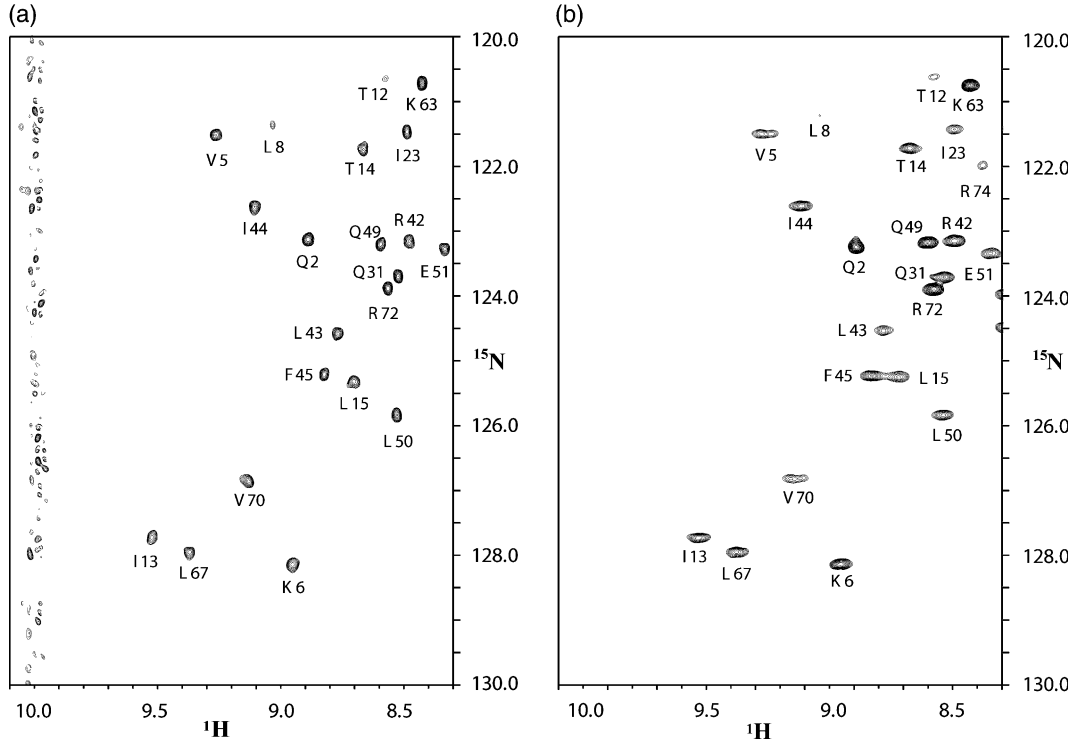

Fig. 1. Comparison of the regions of ubiquitin ^{1}H–^{15}N HSQC spectra recorded in the liquid crystalline phase. Spectrum (b) was measured with a standard NMR probe, which maintains a weak alignment of the molecule. Spectrum (a) was measured for the same sample solution under magic angle spinning at 2.6 kHz. Note that the signals in spectrum (b) are broader than the corresponding signals in spectrum (a) as a result of the residual dipolar couplings among spatially neighboring protons. This confirms that the effective alignment was eliminated under magic angle sample spinning. The noisy line spreading along the ^{15}N dimension at around 10.0 ppm for the ^{1}H frequency is the spinning side band from the large resonance of the water proton. The temperature was fixed at 30 °C. The spectrum for the aligned state was measured using 160 μl of the ^{15}N labeled ubiquitin dissolved in a 7.5% (w/v) bicelle solution poured into a Shigemi microcell (Shigemi). A 40 μl aliquot of the same sample solution was packed into a NanoProbe (Varian) sample tube for spectra obtained under magic angle spinning.

chemical shift changes to the ^{1}H–^{15}N correlation signals (Fig. 1). It should be noted that, in measuring the spectra in liquid crystalline phase, one of the two split ^{2}H lines is used for the frequency lock. Therefore, the chemical shift values in the spectrum include the offset from the center of the two ^{2}H lock signals; this center corresponds to the lock frequency in an isotropic state. To correct properly for the offset in the directly read chemical shift values, two ^{1}H–^{15}N HSQC spectra were collected sequentially with frequency locking to each of the split ^{2}H lines. Thus, the ^{15}N chemical shifts in aligned state that were used in the following analyses were the average of the values read from these sequentially measured spectra. The orientation-dependent ^{15}N chemical shift changes were obtained as $\Delta\delta^{15}N = \delta^{15}N(\text{aniso}) - \delta^{15}N(\text{mas})$, where $\delta^{15}N(\text{aniso})$ is the ^{15}N chemical shift for a residue measured in the aligned state, and $\delta^{15}N(\text{mas})$ is the ^{15}N chemical shift observed under MAS. In Fig. 2, the collected $\Delta\delta^{15}N$ values for ubiquitin along with the corresponding residual dipolar couplings, $^{1}D_{nh}$, obtained from a set of ^{1}H–^{15}N IPAP-HSQC spectra [38] measured with and without MAS are plotted against the residue number. In the present work,

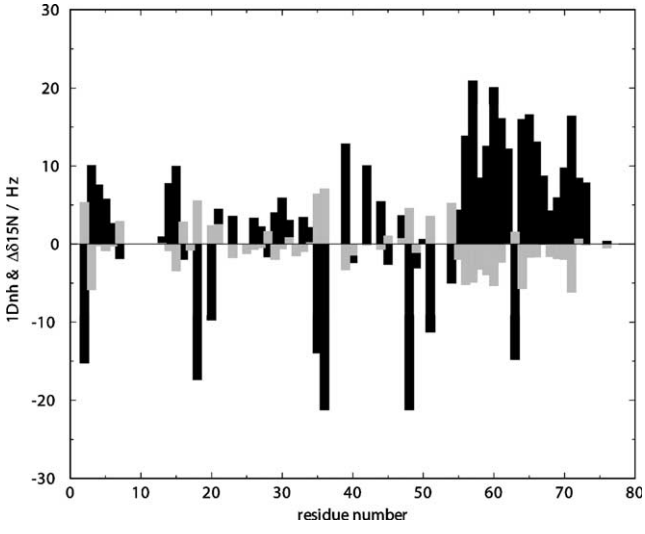

Fig. 2. Residue-by-residue plots of both the residual dipolar couplings, $^{1}D_{nh}$ (black bars), and the orientation-dependent changes to the ^{15}N chemical shifts, $\Delta\delta$ (^{15}N) (gray bars), measured from spectra recorded for ubiquitin in the liquid crystalline phase with and without magic angle sample spinning. For comparison, the $\Delta\delta$ (^{15}N) values are also plotted in units of Hz.

the observed $\Delta\delta^{15}$N values ranged from 0.1207 to −0.1226 ppm. The uncertainty in measuring $\Delta\delta^{15}$N was estimated from the pairwise rms deviation of the ^{15}N chemical shifts in ^{1}H–^{15}N HSQC spectra collected sequentially with a NanoProbe. This value was 6.65 ppb, which corresponds to 0.34 Hz in the present experiment on a 499.84 MHz spectrometer for ^{1}H resonance frequency.

3.2. Determination of the alignment tensor and ^{15}N CSA tensor

The ^{15}N CSA tensor values for ubiquitin were determined according to the procedure described in previous studies [1–3]. To determine the Saupe order matrix [39] that defines the molecular alignment from the residual dipolar couplings, we used the singular value decomposition (SVD) [40]. In the present work, the effect of the internal motion on the scaling of the observed residual dipolar and ^{15}N chemical shift changes was not considered, because it was noted previously that this approximation does not significantly affect the result [3]. In the present analysis, however, to be conservative and avoid the considerable effect of internal motion in the following analysis for ubiquitin, we excluded the values from the flexible terminal residues, 2–11 and 73–76 [41].

The alignment tensor was determined on the basis of the ^{1}H–^{15}N residual dipolar couplings from a set of the IPAP-HSQC spectra [38] measured with and without MAS. For the analysis, we used the 1.8 Å X-ray coordinates of human ubiquitin [42] with protons attached by the program MOLMOL [43]. Zweckstetter and Bax [34] have recently shown that, when fitting dipolar couplings to a high-resolution X-ray crystal structure, structural noise—rather than uncertainties in the measured dipolar couplings—is the primary source of the uncertainty in the alignment tensor values. They also demonstrated that, when considering structural noise as a random NH bond vector distribution in a cone with 5° deviation from the original orientation, the rms deviation between the input and the back-calculated dipolar couplings becomes comparable in size to the experimental observation [34]. Accordingly, in the present analysis, in addition to the uncertainties in the measurements of dipolar couplings and ^{15}N chemical shifts we considered the structural noise.

3.3. Alignment tensor determination

As a prerequisite for the ^{15}N CSA tensor determination, we determined the alignment tensor values under various conditions of noise (Table 1). In these

Table 1
Alignment tensor magnitudes and orientations in ubiquitin[a] determined from experimentally obtained $^{1}D_{nh}$ values with added random noise[b] to reference coordinates containing structural noise[c]

Method	A_{zz} (10^{-4})	A_{yy} (10^{-4})	A_{xx} (10^{-4})	α (deg.)	β (deg.)	γ (deg.)	Rmsd (Hz)[d]	Q[e]
No noise (1)	−12.92	10.60	2.32	72.9	70.4	79.0	2.34	0.165
No noise (2)	−13.09	11.23	2.46	72.9	70.4	79.0	2.34	0.165
Measuring noise (1)[f]	-12.92 ± 0.06	10.60 ± 0.06	2.32 ± 0.04	72.9 ± 0.3	70.4 ± 0.1	79.0 ± 0.2	2.37 ± 0.05	0.167 ± 0.004
Measuring noise (2)	-13.69 ± 0.07	11.23 ± 0.06	2.46 ± 0.04	72.9 ± 0.3	70.4 ± 0.1	79.0 ± 0.2	2.37 ± 0.05	0.167 ± 0.004
Structure noise (1)[g]	-12.82 ± 0.27	10.50 ± 0.28	2.32 ± 0.12	73.1 ± 1.4	70.3 ± 0.9	79.0 ± 1.1	2.75 ± 0.21	0.196 ± 0.017
Structure noise (2)	-13.59 ± 0.29	11.13 ± 0.29	2.46 ± 0.13	73.1 ± 1.4	70.3 ± 0.9	79.0 ± 1.1	2.75 ± 0.21	0.196 ± 0.017
Measuring noise + structural noise (1)[h]	-12.82 ± 0.27	10.50 ± 0.27	2.32 ± 0.14	73.1 ± 1.3	70.3 ± 1.0	78.9 ± 1.1	2.77 ± 0.20	0.197 ± 0.016
Measuring noise + structural noise (2)	-13.59 ± 0.29	11.13 ± 0.29	2.46 ± 0.14	73.1 ± 1.4	70.3 ± 0.9	78.9 ± 1.1	2.77 ± 0.20	0.197 ± 0.016

[a] Using 7.5% bicelles in 95% H_2O, 5% D_2O at 30 °C. The Euler angles α, β, and γ define the alignment tensor relative to the coordinate frame of the 1.8 Å X-ray structure (using the convention of successive rotations around z, y, x axes) [42]. Proton positions were added to the crystal structure using the program MOLMOL [43]. A_{xx}, A_{yy}, and A_{zz} are the principal components of the alignment tensor. Calculations (1) and (2) used $r_{nh} = 0.102$ and 0.104 nm, respectively.

[b] 0.384 Hz rms noise, which corresponds to the uncertainty in the measurement for the residual dipolar couplings, has been added to the experimental values.

[c] A random distribution of each NH bond vector in a cone with 5° tilt angle has been applied prior to the alignment tensor analysis.

[d] Average and standard deviation of the pairwise root mean square deviations between the experimental and back-calculated dipolar couplings obtained from a 1000 time Monte–Carlo simulation.

[e] Average and standard deviation of the quality factor, Q, to the fittings in a 1000 time Monte–Carlo simulation. Quality factor, Q, is defined as $Q = \{\sum_i^N (D_{NHi}^{obs} - D_{NHi}^{pred})^2/N\}^{1/2}/D^{rms}$, where D^{rms} was calculated by considering the non-uniform distribution of the NH-bond vectors in ubiquitin as $D^{rms} = \{D_a^2[4 + 3(D_r/D_a)^2]/5\}^{1/2}$ [44].

[f] A random noise described by a Gaussian distribution with the 0.384 Hz rms was added to the measured dipolar couplings by Monte–Carlo procedure.

[g] The structural uncertainty is simulated by reorienting the NH vectors in a random manner, such that the deviations between the original and final vectors with keeping the nitrogens as origins are randomly distributed in a cone with the tilt angle of 5°.

[h] The random noise addition to the measured dipolar values and the structural noises were simultaneously applied according to the Monte–Carlo procedure.

calculations, a static NH bond length, 1.02 Å, and the vibrationally corrected bond length, 1.04 Å [29], were used. The rms uncertainty in reading the dipolar couplings, 0.39 Hz, produced limited deviation in the alignment tensor values. By contrast, adding structural noise to the X-ray reference coordinates produced significant deviation in the resultant tensors.

In this calculation, in order to retain the reality of the noise simulation, we selected the tensors that yielded close agreement between the experimental uncertainties and the standard errors obtained in the Monte–Carlo simulations. We set the rms deviation margin of acceptance to 3.1 Hz, which corresponds to the addition of a twofold rms uncertainty, 0.39 Hz, to the rms deviation value obtained in the original SVD fit, 2.37 Hz. The fraction of the accepted solution was 76% of the total Monte–Carlo simulations. The obtained alignment tensor values from the structural noise simulation showed approximately 2% uncertainties in both the principal values and the tensor angles to the molecular axis. Simultaneous consideration of uncertainties in the dipolar couplings and structural noise yielded comparable results to those obtained in the calculation based on only structural noise, because the structural noise was the primary source of the uncertainties in the alignment tensor values. In comparing the results with either $r_{nh} = 1.04$ Å or $r_{nh} = 1.02$ Å, the alignment tensor angles were the same, whereas the tensor magnitudes differed from each other (Table 1). In regard to the quality factor [2,44], Q, there was no difference in the fitting between the results obtained with either ^{1}H–^{15}N bond length.

3.4. ^{15}N CSA tensor determination

Fig. 3 defines the orientation of the CSA tensor components σ_{11}, σ_{22}, and σ_{33} relative to the peptide plane represented by the angle β. In this paper, we report the values of chemical shielding tensor, σ, which by convention has the opposite sign of the chemical shift tensor. Using the Saupe order matrix elements determined from the dipolar couplings, we optimized the ^{15}N CSA tensor values, σ_{11}, σ_{22}, σ_{33} and the angle β between the σ_{11} axis and the NH bond by fitting the predicted $\Delta\delta^{15}$N values from the X-ray reference structure to the experimental data. Here, the isotropic chemical shift, $\Delta\sigma_{iso} = (\sigma_{11} + \sigma_{22} + \sigma_{33})/3$, was assumed to be zero, and thus three independent parameters were used as adjustable parameters for fitting. We assumed that all ^{15}N CSA tensor are the same for every residue in the protein; thus, the resultant ^{15}N CSA is the average CSA value. Fig. 4 compares the experimental and the calculated $\Delta\delta^{15}$N with the optimized tensor values. Overall they show a good match, but locally they show subtle differences. These small mismatches are likely to represent the local CSA variation and suggest that the assumption of a uniform CSA value is not completely perfect. Table 2 lists the obtained average ^{15}N CSA tensor values from the present experiment. For comparison, previously reported values from the solid-state NMR experiments are also listed in Table 2.

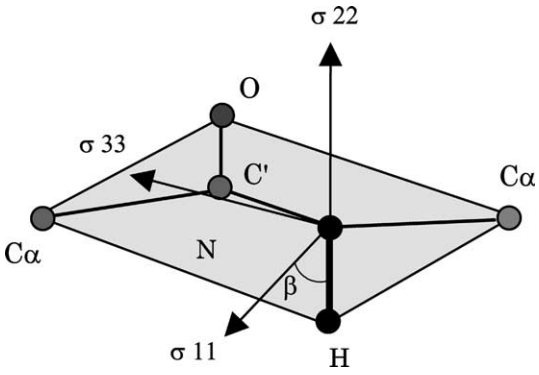

Fig. 3. Definition of the principal coordinate system for ^{15}N chemical shift anisotropy on the peptide plane.

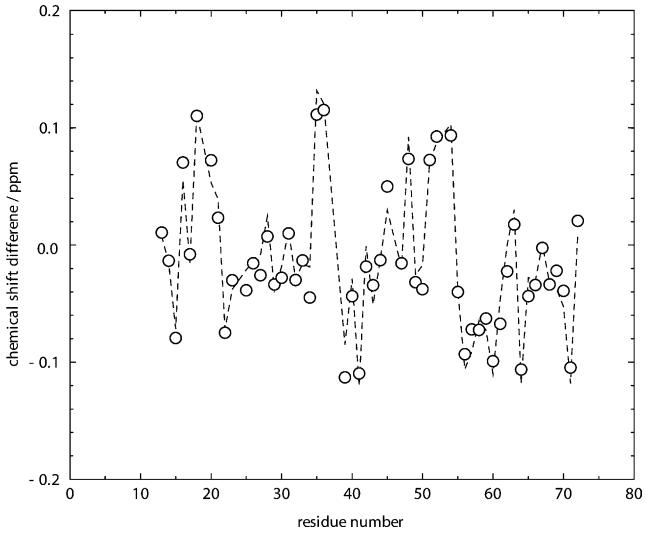

Fig. 4. Plots of the observed orientation-dependent ^{15}N chemical shift changes (dotted line) and the values calculated (open circles) with the optimized ^{15}N CSA tensor values and the 1.8-Å X-ray coordinate of ubiquitin [42] with proton attachment by the program MOLMOL [43].

The ^{15}N CSA values were calculated with two ^{1}H–^{15}N bond lengths, 1.02 Å for the static bond length and 1.04 Å for the vibrationally corrected value [29]. For the calculations, the experimental uncertainties in reading the dipolar couplings, 0.39 Hz, and the ^{15}N chemical shift, 6.7 ppb (0.34 Hz), were considered in addition to the structural noise in the reference X-ray structure. As in the case of the alignment tensor determination, these noises were incorporated into the calculation by Monte–Carlo simulation. The uncertainties in the resultant CSA values were elucidated as a standard deviation in the fraction of the accepted solution. The selection for the solution was based on the consistency between the back-calculated and input dipolar

Table 2
Average backbone ^{15}N CSA tensor magnitude and orientation in ubiquitin determined in the present work[a] with summary of the ^{15}N CSA tensors determined from various samples[b]

Sample	σ_{11} (ppm)	σ_{22} (ppm)	σ_{33} (ppm)	$\Delta\sigma$[c] (ppm)	η[d]	β (deg.)	Q[e]	Rmsd (ppm)[f]	Ref.
^{15}N–ubiquitin (1)[g]	−107.2	43.8	63.4	−160.8	0.18	18.7	0.21	0.013	Present work
^{15}N–ubiquitin (2)	−101.1	41.4	59.8	−151.7	0.18	18.7	0.21	0.013	Present work
Monte–Carlo sim. (1)[h]	-108.0 ± 2.9	44.2 ± 1.9	63.8 ± 1.9	-162.0 ± 4.3	0.18 ± 0.02	18.6 ± 0.5	0.24 ± 0.02	0.015 ± 0.001	Present work
Monte–Carlo sim. (2)	-101.9 ± 2.7	41.7 ± 1.8	60.2 ± 1.8	-152.9 ± 4.1	0.18 ± 0.02	18.6 ± 0.5	0.24 ± 0.02	0.015 ± 0.001	Present work
^{15}N-lysozyme	−116.3	49.4	66.9	−174.4	0.15	18.7			[1]
$^{2}H/^{13}C/^{15}N$–ubiquitin	−108.3	43.9	64.5	−162.5	0.19	20			[3]
^{15}N–Gly collagen powder	−112.5	43.9	68.6	−168.8	0.22	24.5			[17]
^{2}H–^{15}N–Gly collagen	−106.8	42.4	64.4	−160.2	0.21	23			[15]
$AcGlyAlaNH_2$	−109.7	34.6	75.1	−164.6	0.37	17.6			[19]
$AcGlyTyrNH_2$	−96.5	35.7	60.7	−144.7	0.26	19.6			[19]
GlyGlyHCl	−101.0	49.2	51.7	−151.5	0.02	18.6			[19]
$AcGlyGlyNH_2$	−105.0	40.8	64.3	−157.6	0.22	17.6			[19]
Boc–$(Gly)_2$$^{15}N$–Gly–OBz	−109.6	51.3	58.3	−164.4	0.06	22			[14]
$GlyGlyHClH_2O$ (crystal)	−100.0	44.8	55.4	−150.3	0.11	21.3			[13]
$GlyGlyHClH_2O$ (powder)	−98.8	46.6	52.2	−148.2	0.06	25			[21]
Ala–^{15}N–Len	−97.7	45.9	51.8	−146.5	0.06	17			[23]
Average[i]	-103.8 ± 5.7	43.5 ± 5.4	60.3 ± 5.4	-155.3 ± 8.2	0.16 ± 0.11	20.6 ± 3.0			

[a] σ_{11}, σ_{22}, σ_{33} values are evaluated the isotropic chemical shift, σ_{iso}, being zero.

[b] All principal values of the chemical shifts were re-evaluated under the assumption of $\sigma_{iso} = 0.0$ from the reported values in the literatures.

[c] $\Delta\sigma = \sigma_{11} - (\sigma_{22} + \sigma_{33})/2$.

[d] $\eta = [(\sigma_{int} - \sigma_{min})/\sigma_{max}]$, where the subscripts maximum(max), minimum(min), and intermediate(int) refer to the absolute magnitudes of σ_{11}, σ_{22}, σ_{33}.

[e] Quality factor, Q, defines the value $\sum_i^N (\Delta\delta_N^{obs.} - \Delta\delta_N^{pred.})^2 / \sum_i^N (\Delta\delta_N^{obs.})^2$ [3].

[f] Pairwise root mean square deviation between best-fitted and observed $\Delta\delta_N$.

[g] Calculations (1) and (2) used $r_{nh} = 0.102$ and 0.104 nm, respectively.

[h] The random noise was added to the measured dipolar couplings and the structures used for the calculation contained structural noise allowing the random reorientation of the NH vectors in a cone of 5° tilt angle. Calculations (1) and (2) used $r_{nh} = 0.102$ and 0.104 nm, respectively. The experimentally evaluated rms noises were added to the measured values with assuming a Gaussian noise distribution by the Monte–Carlo procedure; the applied rms noises were 0.384 Hz and 6.65 ppb (0.336 Hz) for the dipolar couplings and chemical shifts, respectively.

[i] Average and rmsd values of the cited ^{15}N CSA tensor values determined by the solid-state NMR experiments.

couplings; the margin of acceptance was set to 3.1 Hz as used in the alignment tensor determination described above.

The $\Delta\sigma$ values obtained in the present analyses were -162.0 and -152.9 ppm for $r_{nh} = 1.02$ Å and 1.04 Å, respectively. And the uncertainties in the CSA tensor values were around 3%. These values are in good agreement with data from solid-state NMR experiments. The average $\Delta\sigma$ value from the listed representative solid-state data was -155.3 ± 8.2 ppm (Table 2). The present $\Delta\sigma$ values with the two ^1H–^{15}N bond lengths were both within a standard deviation of the listed solid-state $\Delta\sigma$ values. This was also the case for the values of η and β.

Boyd and Redfield [1] have evaluated the $\Delta\sigma$ value using different X-ray structures for lysozyme as the reference coordinates. They selected 10 structures that gave Q factors below 0.22, and their calculation produced the following uncertainties in the resultant ^{15}N CSA tensors: $\Delta\sigma = -173.6 \pm 2.1$ ppm, $\eta = 0.16 \pm 0.01$, and $\beta = 18.2 \pm 0.8°$ by assuming $r_{nh} = 1.04$ Å [1]. We note that the uncertainties in their ^{15}N CSA tensor are close to those estimated in the present Monte–Carlo simulation. This fact supports the previous proposal that the X-ray coordinates should be considered to include structural noise represented by a Gaussian random distribution of each ^1H–^{15}N bond vector in a cone with deviation angle of 5° [34].

In addition to the uncertainties in measurement and reference structure, we also considered other possible systematic errors in the present experiment. At this stage, the high-resolution MAS experiment has an intrinsic, unavoidable source of systematic error in measuring $\Delta\delta^{15}N$, because in the experiment with a NanoProbe, we cannot measure a high-resolution spectrum without sample spinning. MAS above a significant spin rate diminishes the demagnetization field from a sample tube in a coil, which thereby destroys the magnetic field homogeneity around the sample inclined to the magnetic field [45]. Thus, without sample spinning, not enough field homogeneity is attained around the sample in a magic angle probe by the usual shimming procedure. In our spectrometer setup, a sample spin rate above 1.5 kHz was necessary to gain enough field homogeneity to record high-resolution spectra. Because of the difficulty in shimming for a magic angle probe without rapid sample spin [45], we had to switch the NanoProbe to an ordinary probe to collect the spectra of the weakly aligned protein. Owing to the different architectures of these two NMR probes, the efficiency of sample cooling by air flow is likely to differ between experiments with the two probes. In the NanoProbe experiment, the total sample volume was 40 μl as compared with the 160 μl used in ordinary probe experiments; in addition, the air flow in a NanoProbe was much faster than that in the ordinary probe, because in a NanoProbe the applied air is simultaneously used for rapid sample spin, typically at 2.6 kHz, and for sample cooling. Thus, even though the same probe temperature is set on the console, the effective sample temperature will change during radiofrequency pulsing, owing to different sample heating between the experiments with a NanoProbe and an ordinary probe. To avoid unwanted changes in the sample temperatures during the experiments, before starting all experiments we carefully adjusted the temperature on both probes to keep the effective sample temperature the same by monitoring the chemical shift difference between the two peaks in an ethylene glycol spectrum [46]. The average pairwise ^{15}N shift difference, $\delta^{15}N$ (NanoProbe) $- \delta^{15}N$ (ordinary probe) and its standard deviation on all residues used for the ^{15}N CSA analysis were -0.0051 ± 0.0061 ppm. This is almost the size of the rms error in the chemical shift values, thus, there seems to be a marginal offset in the chemical shifts between the experiments with a NanoProbe spectra and those with an ordinary probe. This ^{15}N systematic drift probably comes from the different cooling efficiencies in the probes in spite of the careful temperature setting prior to the experiments. Despite that fact that the marginal size of the drift in the ^{15}N chemical shifts was less than the rms measurement error, 6.1 ppb, to determine its effect on the resultant CSA value, we recalculated the ^{15}N CSA tensor by imposing this offset, -0.0051 ppm, on the experimental $\Delta\delta^{15}N$. The re-evaluated CSA values were -154.7 and -164.0 ppm for $r_{nh} = 1.04$ and 1.02 Å, respectively. Both of them were smaller than the original $\Delta\sigma$ values, whereas the fitting qualities in both cases were the same as in the original dataset; the rms deviation between the experimental and the back-calculated $\Delta\delta^{15}N$ was 0.013 ppm ($Q = 0.21$) in either case. From this recalculation, we could demonstrate that even a very small systematic chemical shift offset to the observed $\Delta\delta^{15}N$ can alter the $\Delta\sigma$ value by about 1%. Thus, this result indicates that systematic drift in the $\Delta\delta^{15}N$ values, which happens even when there are only subtle changes in experimental conditions, has to be treated carefully in discussing the approximately 6% difference in $\Delta\sigma$ values observed between solid-state and liquid-state NMR experiments.

4. Conclusions

In summary, we have shown a new approach for obtaining the ^{15}N CSA tensor values in liquid-state NMR experiments. In the present approach, magic angle sample spinning, MAS, was used. In this MAS based experiment, we can switch the ordered state of proteins to an isotropic state by simply applying sample rotation and keeping all other conditions the same. The chemical shift is extremely sensitive to the changes in experi-

mental conditions including temperature, pH and the state of the co-solutes, i.e., bicelles or micelles; thus, the present approach yields accurate orientation-dependent ^{15}N chemical shift changes that are the basis for the ^{15}N CSA tensor determination.

In the present work, we considered the structural noise that intrinsically exists in the X-ray reference structure [34], in addition to the errors in measuring the dipolar couplings and chemical shifts. The elucidated $\Delta\sigma$ and β values in the present work were $\Delta\sigma = -162.0 \pm 4.3$ ppm, $\beta = 18.6 \pm 0.5°$, and $\Delta\sigma = -152.9 \pm 4.1$ ppm, $\beta = 18.6 \pm 0.5°$ with the assumption of $r_{nh} = 1.02$ Å and $r_{nh} = 1.04$ Å, respectively. Both of these values were consistent with the mean $\Delta\sigma$, β values among the representative solid-state values listed in Table 2; -155.3 ± 8.2 ppm, $\beta = 20.6 \pm 3.0°$. And the present $\Delta\sigma$ and β values, which are determined with the static ^1H–^{15}N bond length of 1.02 Å, were fairly consistent with values obtained from magnetic field alignment [4], $\Delta\sigma = -168 \pm 20$ ppm, $\beta = 13 \pm 5°$, and those obtained from ^{15}N spin relaxation analyses at multiple fields [25], $\Delta\sigma = -157 \pm 19$ ppm, $\beta = 15.7 \pm 5°$.

In this study, we also demonstrated that the apparently marginal systematic error in the observed $\Delta\delta^{15}N$ also causes a 1% decrease in the calculated $\Delta\sigma$ value; from −162.0 to −164.0 ppm. Therefore, the accumulation of systematic errors of a few percent may induce significant biases in the resultant $\Delta\sigma$ values. The systematic errors in experimental values may become apparent, for example, in different solute states, i.e., bicelle or micelle, and/or in different protein–phospholipid contacts at shifted temperature. These small differences do not seem to be readily resolved in temperature shift experiments to measure $\Delta\sigma^{15}N$ [1,3], in which the $\Delta\delta^{15}N$ values are extracted after correcting the intrinsic temperature-induced chemical shift changes. These poorly resolved errors in the temperature-shift experiments may explain, in part, the approximately 6% difference in the $\Delta\sigma$ values between the temperature shift experiments [1,3] and those obtained in the present MAS based experiment. We may need further careful analyses to see the significance of the difference in the $\Delta\sigma$ values determined by the similar experiments based on $\Delta\delta^{15}N$.

The high-resolution MAS based experiment described here would provide a good alternative way to determine accurate CSA tensor values for other nuclei, if further hardware modifications are made to the probe. With the currently available NanoProbe we could not vary the spin angle against the magnetic field; that is, the variable angle range was limited to within a few degrees around the magic angle. If the variable angle sample spinning (VASS) experiment [30–33] could be achieved with a high-resolution MAS probe like a NanoProbe, we would be able to obtain much accurate CSA values by collecting the orientation-dependent changes to chemical shifts and the dipolar couplings at various angles, thereby tuning the anisotropic spin interaction in the bicelle medium to various degrees [32,33].

Acknowledgments

We are grateful to Drs. Katsuhiko Kushida and Jun Ashida (Varian Technologies Japan) for lending us the instruments at the initial stage of the present work and for useful discussions. This research was partly supported by the ministry of education, culture, sports, science and technology, Grant-in-Aid for Scientific Research on Priority Areas (12034209). This work was also supported by the Japan New Energy and Industrial Technology Development Organization (NEDO). S.T. thanks the Sumitomo Foundation, the Inamori Foundation and Novartis Foundation for financial support to progress the present research.

References

[1] J. Boyd, C. Redfield, Characterization of ^{15}N chemical shift anisotropy from orientation-dependent changes to ^{15}N chemical shifts in dilute bicelle solutions, J. Am. Chem. Soc. 121 (1999) 7441–7442.

[2] G. Cornilescu, J. Marquardt, M. Ottiger, A. Bax, Validation of protein structure from anisotropic carbonyl chemical shifts in a dilute liquid crystalline phase, J. Am. Chem. Soc. 120 (1998) 6836–6837.

[3] G. Cornilescu, A. Bax, Measurement of proton, nitrogen, and carbonyl chemical shielding anisotropies in a protein dissolved in a dilute liquid crystalline, J. Am. Chem. Soc. 122 (2000) 10143–10154.

[4] M. Ottiger, N. Tjandra, A. Bax, Magnetic field dependent amide ^{15}N chemical shifts in a protein–DNA complex resulting from magnetic ordering in solution, J. Am. Chem. Soc. 119 (1997) 9825–9830.

[5] M.W. Fischer, A. Majumdar, E.R. Zuiderweg, Protein NMR relaxation: theory, applications and outlook, Prog. NMR spectrosc. 33 (1998) 207–272.

[6] M.W. Fischer, L. Zeng, A. Majumdar, E.R. Zuiderweg, Characterizing semilocal motions in proteins by NMR relaxation studies, Proc. Natl. Acad. Sci. USA 95 (1998) 8016–8019.

[7] D. Fushman, D. Cowburn, The effect of noncollinearity of ^{15}N–^1H dipolar and ^{15}N CSA tensors and rotational anisotropy on ^{15}N relaxation, CSA/dipolar cross correlation, and TROSY, J. Biomol. NMR 13 (1999) 139–147.

[8] S.F. Lienin, T. Bremi, B. Brutscher, R. Bruschweiler, R.R. Ernst, Anisotropic intramolecular backbone dynamics of ubiquitin characterized by NMR relaxation and MD computer simulation, J. Am. Chem. Soc. 120 (1998) 9870–9879.

[9] C. Scheurer, N.R. Skrynnikov, S.F. Lienin, S.K. Straus, R. Bruschweiler, R.R. Ernst, Effects of dynamics and environment on ^{15}N chemical shielding anisotropy in proteins. A combination of density functional theory, molecular dynamics simulation, and NMR relaxation, J. Am. Chem. Soc. 121 (1999) 4242–4251.

[10] R. Ghose, K. Huang, J.H. Prestegard, Measurement of cross correlation between dipolar coupling and chemical shift anisotropy in the spin relaxation of ^{13}C, ^{15}N-labeled proteins, J. Magn. Reson. 135 (1998) 487–499.

[11] H. Schwalbe, T. Carlomagno, M. Hennig, J. Junker, B. Reif, C. Richter, C. Griesinger, Cross-correlated relaxation for

measurement of angles between tensorial interactions, Methods Enzymol. 338 (2001) 35–81.
[12] T.M. Duncan, A Compilation of Chemical Shift Anisotropies, Farragut Press, Madison, 1990.
[13] G.S. Harbison, L.W. Jelinski, R.E. Stark, D.A. Torchia, J. Herzfeld, R.G. Griffin, Chemical shift and ^{15}N–^{13}C dipolar tensors for the peptide bond in 1-^{13}C-glycyl-^{15}N-glycine hydrochloride monohydrate, J. Magn. Reson. 60 (1984) 79–82.
[14] Y. Hiyama, C.H. Niu, J.V. Silverton, A. Bavoso, D.A. Torchia, Determination of ^{15}N chemical shift tensor via ^{15}N–^{2}H dipolar coupling in Boc-glycylglycyl [^{15}N glycine]benzyl ester, J. Am. Chem. Soc. 110 (1988) 2378–2383.
[15] L.W. Jelinski, D.A. Torchia, $^{13}C/^{1}H$ high power double magnetic resonance investigation of collagen backbone motion in fibrils and in solution, J. Mol. Biol. 133 (1979) 45–65.
[16] D.K. Lee, A. Ramamoorthy, A simple one-dimensional solid-state NMR method to characterize the nuclear spin interaction tensors associated with the peptide bond, J. Magn. Reson. 133 (1998) 204–206.
[17] D.K. Lee, R.J. Wittebort, A. Ramamoorthy, Characterization of ^{15}N chemical shift and ^{1}H–^{15}N dipolar coupling interactions in a peptide bond of uniaxially oriented and polycrystalline samples by one-dimensional dipolar chemical shift solid-state NMR spectroscopy, J. Am. Chem. Soc. 120 (1998) 8868–8874.
[18] T.G. Oas, C.J. Hartzell, T.J. McMahon, G.P. Drobny, F.W. Dahlquist, The carbonyl carbon-13 chemical shift tensors of five peptides determined from nitrogen-15 dipole-coupled chemical shift powder patterns, J. Am. Chem. Soc. 109 (1987) 5956–5962.
[19] T.G. Oas, C.J. Hartzell, F.W. Dahlquist, G.P. Drobny, The amide nitrogen-15 chemical shift tensors of four peptides determined from carbon-13 dipole-coupled chemical shift powder patterns, J. Am. Chem. Soc. 109 (1987) 5962–5966.
[20] A. Ramamoorthy, C.H. Wu, S.J. Opella, Experimental aspects of multidimensional solid-state NMR correlation spectroscopy, J. Magn. Reson. 140 (1999) 131–140.
[21] J.E. Roberts, G.S. Harbison, M.G. Munowitz, J. Herzfeld, R.G. Griffin, Measurement of heteronuclear bond distances in polycrystalline solids by solid-state NMR techniques, J. Am. Chem. Soc. 109 (1987) 4163–4169.
[22] Q. Teng, M. Iqbal, T.A. Cross, Determination of the carbon-13 chemical shift and nitrogen-14 electric field gradient tensor orientations with respect to the molecular frame in a polypeptide, J. Am. Chem. Soc. 114 (1992) 5312–5321.
[23] C.H. Wu, A. Ramamoorthy, L.M. Gierasch, S.J. Opella, Simultaneous characterization of the amide ^{1}H chemical shift, ^{1}H–^{15}N dipolar, and ^{15}N chemical shift interaction tensors in a peptide bond by three-dimensional solid-state NMR spectroscopy, J. Am. Chem. Soc. 117 (1995) 6148–6149.
[24] D. Fushman, D. Cowburn, Model-independent analysis of ^{15}N chemical shift anisotropy from NMR relaxation data. Ubiquitin as a test example, J. Am. Chem. Soc. 120 (1998) 7109–7110.
[25] D. Fushman, N. Tjandra, D. Cowburn, An approach to direct determination of protein dynamics from ^{15}N NMR relaxation at multiple fields, independent of variable ^{15}N chemical shift anisotropy and chemical exchange contribution, J. Am. Chem. Soc. 121 (1999) 8577–8582.
[26] D. Fushman, D. Cowburn, Nuclear magnetic resonance relaxation in determination of residue-specific ^{15}N chemical shift tensors in proteins in solution: protein dynamics, structure, and applications of transverse relaxation optimized spectroscopy, Methods Enzymol. 339 (2001) 109–126.
[27] C.D. Kroenke, M. Rance, A.G. Palmer III, Variability of the ^{15}N chemical shift anisotropy in *Escherichia coli* ribonuclease H in solution, J. Am. Chem. Soc. 121 (1999) 10119–10125.
[28] N. Tjandra, A. Szabo, A. Bax, Protein backbone dynamics and ^{15}N chemical shift anisotropy from quantitative measurement of relaxation interference effects, J. Am. Chem. Soc. 118 (1996) 6986–6991.
[29] M. Ottiger, A. Bax, Determination of relative N–H^N, N–C', C^a–C', and C^a–H^a effective bond lengths in a protein by NMR in a dilute liquid crystalline phase, J. Am. Chem. Soc. 120 (1998) 12334–12341.
[30] J. Courtieu, D.W. Alderman, D.M. Grant, J.P. Bayles, Director dynamics and NMR applications of nematic liquid crystals spinning at various angles from the magnetic field, J. Chem. Phys. 77 (1982) 723–730.
[31] J. Courtieu, J.P. Bayles, B.M. Fung, Variable angle sample spinning NMR in liquid crystals, Prog. NMR spectrosc. 26 (1994) 141–169.
[32] F. Tian, J.A. Losonczi, M.W. Fischer, J.H. Prestegard, Sign determination of dipolar couplings in field-oriented bicelles by variable angle sample spinning (VASS), J. Biomol. NMR 15 (1999) 145–150.
[33] G. Zandomeneghi, M. Tomaselli, J.D. van Beek, B.H. Meier, Manipulation of the director in bicellar mesophases by sample spinning: a new tool for NMR spectroscopy, J. Am. Chem. Soc. 123 (2001) 910–913.
[34] M. Zweckstetter, A. Bax, Evaluation of uncertainty in alignment tensors obtained from dipolar couplings, J. Biomol. NMR 23 (2002) 127–137.
[35] A. Bax, N. Tjandra, High-resolution heteronuclear NMR of human ubiquitin in an aqueous liquid crystalline medium, J. Biomol. NMR 10 (1997) 289–292.
[36] A. Bax, G. Kontaxis, N. Tjandra, Dipolar couplings in macromolecular structure determination, Methods Enzymol. 339 (2001) 127–174.
[37] M. Ottiger, A. Bax, Characterization of magnetically oriented phospholipid micelles for measurement of dipolar couplings in macromolecules, J. Biomol. NMR 12 (1998) 361–372.
[38] M. Ottiger, F. Delaglio, A. Bax, Measurement of J and dipolar couplings from simplified two-dimensional NMR spectra, J. Magn. Reson. 131 (1998) 373–378.
[39] A. Saupe, Recent results in the field of liquid crystals, Angew. Chem., Int. Ed. Engl. 7 (1968) 97–112.
[40] J.A. Losonczi, M. Andrec, M.W. Fischer, J.H. Prestegard, Order matrix analysis of residual dipolar couplings using singular value decomposition, J. Magn. Reson. 138 (1999) 334–342.
[41] N. Tjandra, H. Kuboniwa, H. Ren, A. Bax, Rotational dynamics of calcium-free calmodulin studied by ^{15}N-NMR relaxation measurements, Eur. J. Biochem. 230 (1995) 1014–1024.
[42] S. Vijay-Kumar, C.E. Bugg, W.J. Cook, Structure of ubiquitin refined at 1.8 Å resolution, J. Mol. Biol. 194 (1987) 531–544.
[43] R. Koradi, M. Billeter, K. Wuthrich, MOLMOL: a program for display and analysis of macromolecular structures, J. Mol. Graph. 14 (1996) 51–55.
[44] G.M. Clore, M.R. Starich, A.M. Gronenborn, Measurement of residual dipolar couplings of macromolecules aligned in the nematic phase of a colloidal suspension of rod-shaped viruses, J. Am. Chem. Soc. 120 (1998) 10571–10572.
[45] T.M. Barbara, Cylindrical demagnetization fields and microprobe design in high-resolution NMR, J. Magn. Reson. A 109 (1994) 265–269.
[46] S. Braun, H.-O. Kalinowski, S. Berger, 100 More Basic NMR Experiments, VCH, New York, 1996.
[47] D.M. Schneider, M.J. Dellwo, A.J. Wand, Fast internal main-chain dynamics of human ubiquitin, Biochemistry 31 (1992) 3645–3652.
[48] J. Cavanagh, W.J. Fairbrother, A.G. Palmer III, N.J. Skelton, Protein NMR, Academic Press, San Diego, 1996.
[49] J.A. Losonczi, J.H. Prestegard, Improved dilute bicelle solutions for high-resolution NMR of biological macromolecules, J. Biomol. NMR 12 (1998) 447–451.

[50] M. Ottiger, A. Bax, Bicelle-based liquid crystals for NMR-measurement of dipolar couplings at acidic and basic pH values, J. Biomol. NMR 13 (1999) 187–191.
[51] F. Delaglio, S. Grzesiek, G.W. Vuister, G. Zhu, J. Pfeifer, A. Bax, NMRPipe: a multidimensional spectral processing system based on UNIX pipes, J. Biomol. NMR 6 (1995) 277–293.
[52] D.S. Garrett, R. Powers, A.M. Gronenborn, G.M. Clore, A common sense approach to peak picking in two-, three-, and four-dimensional spectra using automatic computer analysis of contour diagrams, J. Magn. Reson. 95 (1991) 214–220.
[53] A.C. Wang, A. Bax, Determination of the backbone dihedral angle phi in human ubiquitin from reparametrized empirical Karplus equations, J. Am. Chem. Soc. 118 (1996) 2483–2494.
[54] W.H. Press, S.A. Teukolsky, W.T. Vetterling, B.P. Flannery, Numerical Recipes in C, second ed., Cambridge university press, New York, 1992.